applied sciences

MDPI

Article

Graphene Nanoplatelets: In Vivo and In Vitro Toxicity, Cell Proliferative Activity, and Cell Gene Expression

Beatriz Salesa [1], Alberto Tuñón-Molina [1], Alba Cano-Vicent [1], Marcelo Assis [2], Juan Andrés [2] and Ángel Serrano-Aroca [1,*]

[1] Biomaterials and Bioengineering Lab, Centro de Investigación Traslacional San Alberto Magno, Universidad Católica de Valencia San Vicente Mártir, c/Guillem de Castro 94, 46001 Valencia, Spain; beatriz.salesa@ucv.es (B.S.); alberto.tunon@ucv.es (A.T.-M.); alba.cano@mail.ucv.es (A.C.-V.)

[2] Department of Physical and Analytical Chemistry, University Jaume I (UJI), 12071 Castellon, Spain; marcelostassis@gmail.com (M.A.); andres@qfa.uji.es (J.A.)

* Correspondence: angel.serrano@ucv.es; Tel.: +34-963637412 (ext. 5256)

Abstract: Multi-layer graphene (2–10 layers), also called graphene nanoplatelets (GNPs), is a carbon-based nanomaterial (CBN) type with excellent properties desirable for many biomedical applications. Despite the promising advantages reported of GNPs, nanoscale materials may also present a potential hazard to humans. Therefore, in this study, the in vivo toxicity of these nanomaterials at a wide range of concentrations from 12.5 to 500 μg/mL was evaluated in the *Caenorhabditis elegans* model for 24 h (acute toxicity) and 72 h (chronic toxicity). Furthermore, their in vitro toxicity (from 0 to 10 μg/mL for 12 and 24 h), proliferative activity at 72 and 96 h, and their effect on the expression of thirteen genes in human keratinocytes HaCaT cells were studied. The physico-chemical and morphological aspects of the GNPs used in this study were analyzed by Raman scattering spectroscopy, electron microscopy, zeta potential as a function of pH, and particle size measurements by dynamic light scattering. The results of this study showed that GNPs showed in vivo non-toxic concentrations of 25 and 12.5 μg/mL for 24 h, and at 12.5 μg/mL for 72 h. Moreover, GNPs present time-dependent cytotoxicity (EC_{50} of 1.142 μg/mL and 0.760 μg/mL at 12 h and 24 h, respectively) and significant proliferative activity at the non-toxic concentrations of 0.005 and 0.01 μg/mL in the HaCaT cell line. The gene expression study showed that this multi-layer-graphene is capable of up-regulating six of the thirteen genes of human keratinocytes (*SOD1*, *CAT*, *TGFB1*, *FN1*, *CDH1*, and *FBN*), two more genes than other CBNs in their oxidized form such as multi-layer graphene oxide. Therefore, all these results reinforce the promising use of these CBNs in biomedical fields such as wound healing and skin tissue engineering.

Keywords: graphene nanoplatelets; human keratinocytes; toxicity; proliferative activity; gene expression; *Caenorhabditis elegans*

Citation: Salesa, B.; Tuñón-Molina, A.; Cano-Vicent, A.; Assis, M.; Andrés, J.; Serrano-Aroca, Á. Graphene Nanoplatelets: In Vivo and In Vitro Toxicity, Cell Proliferative Activity, and Cell Gene Expression. *Appl. Sci.* **2022**, *12*, 720. https://doi.org/10.3390/app12020720

Academic Editor: Morgan Hamon

Received: 13 December 2021
Accepted: 10 January 2022
Published: 12 January 2022

1. Introduction

Carbon-based nanomaterials (CBNs) are very promising functional materials with many advanced biomedical applications, including medical imaging and nanotherapeutics [1–3]. In fact, CBNs have been recently proposed as next-generation antimicrobials to combat infectious diseases such as the current Coronavirus disease 2019 (COVID-19) because they have unique biological properties such as antimicrobial activity against a broad range of microorganisms, the capacity of inducing tissue regeneration, and low risk of antimicrobial resistance [4]. The antimicrobial mechanism of CBNs is usually attributed to a combination of physical and chemical processes such as membrane structure disruption, microorganism entrapment, electron transfer, and/or oxidative stress by the action of reactive oxygen species (ROS) [5]. Moreover, they possess many other excellent physical and biological properties such as high thermal and electrical conductivity, excellent mechanical performance, immunomodulatory potential and can be combined with stem cells

in regenerative medicine [4,6–10]. CBNs are a broad class of materials that involve single layer graphene, few-layer composed of 2–5 layers of graphene sheets packed together, and multi-layer graphene (2–10 layers), also called graphene nanoplatelets (GNPs) [11]. All these types of CBNs can also be produced in their oxidized form and have shown many different biological properties in terms of cytotoxicity, proliferative activity, and capacity of up-regulating genes in human keratinocytes HaCaT cells. Thus, CBNs such as few-layer graphene have shown to be less cytotoxic than few-layer graphene oxide (GO) in HaCaT cells [12]. Other CBNs in their oxidized form such as multi-layer GO, which contain hydroxyl (-OH), carboxyl (-COOH) and epoxy (C–O–C) groups on the basal planes and at the edges of the GO nanosheets, has shown to be much more cytotoxic than few-layer GO, which has shown very weak cytotoxicity in a broad range of cell lines, including glioma and human skin HaCaT cells [13]. Furthermore, few-layer GO have shown anti-proliferative effects in several cell lines including the HaCaT cell line in contrast to multi-layer GO, which showed similar proliferative activity to an epidermal growth factor (EGF) [13]. In that study, multi-layer GO showed to be able to up-regulate four genes (*CAT*, *TGFB1*, *FN1*, and *CDH1*) that are relevant in biomedicine [13]. Another CBN in the form of carbon filamentous hollow materials has recently been shown to be capable of up-regulating many more genes than other types of nanomaterials, silver nanoparticles, and thus showing the great potential of CBNs in the biomedical field [14].

GNPs have shown excellent physical and biological properties such as antimicrobial activity [15,16]. Despite the promising advantages of GNPs in the biomedical field, nanoscale materials may also present a potential hazard to human health, requiring extensive investigation into their in vitro and in vivo toxicity to guarantee safe use of this emerging nanotechnology. Thus, in this study, we analyze the cytotoxicity, proliferative activity, and the effect of GNPs on the expression of thirteen genes (*SOD1*, *CAT*, *MMP1*, *TGFB1*, *GPX1*, *FN1*, *HAS2*, *LAMB1*, *LUM*, *CDH1*, *COL4A1*, *FBN*, and *VCAN*) in human keratinocytes HaCaT cells. These genes were chosen because they are highly associated with biochemical processes, including oxidative stress, extracellular matrix regulation, and the synthesis of proteins to maintain and repair tissues, which can provide valuable information to know the potential use of these CNBs in biomedical applications such as wound healing and skin tissue engineering. Furthermore, the toxicity of this advanced technology will be evaluated using the nematode *Caenorhabditis elegans* in vivo model, which is a well-establish animal model with digestive, reproductive, endocrine, sensory and neuromuscular systems frequently used to study human development and disease [17,18].

2. Materials and Methods

2.1. Materials

Graphene nanoplatelets, GNPs, xGnP® (2 µm particle size, surface area 500 m^2/g, <2 µg) were purchased from Sigma-Aldrich (Buchs, Switzerland). Fetal bovine serum (FBS), low glucose Dulbecco's modified Eagle medium (DMEM), peniciline-streptomicine (P/S), L-glutamine, and epidermal growth factor (EGF) were supplied by Life Technologies (Gibco, Karlsruhe, Germany). RNA purification kit and PrimeScript™ RT Reagent kit (perfect real time) were obtained from Norgen (Thorold, Canada) and Takara Bio Inc. (Kusatsu, Japan), respectively.

2.2. Material Characterization

Transmission electron microscopy (TEM) was performed on a Jeol 2100 microscope, operated at 200 kV. The GNPs were dispersed in water under sonication for 5 min. After this procedure, the carbon and copper sample holder (grid) were immersed in this solution and dried at room temperature. Raman scattering spectroscopy was performed on a JASCO spectrometer coupled to a CCD detector. This analysis was performed with an argon-ion laser with a wavelength of 514.5 nm operated at a power of 200 mW. The Zetasizer NanoZS equipment was used to obtain the zeta potential (ζ), dynamic light scattering (DLS), and polydispersity index (PdI). For the pH variation (pH = 3, 5, 7, 10, and 12) used in the

zeta potential measurements, the pH was adjusted with HNO_3 (Synth, 70%) and NH_4OH (Synth, 24%). The particle hydrodynamic size of the GNPs was evaluated by DLS in water and in the same DMEM used in this study to determine the biological properties of these nanomaterials.

2.3. Culture Maintenance

HaCaT cell line (immortalized human keratinocytes), provided by the Medical Research Institute Hospital La Fe, was used to perform in vitro assays. Cells were cultured in a humidified atmosphere inside a CO_2 incubator at 37 °C, using for their growth and maintenance low glucose DMEM, supplemented with P/S 1%, L-glutamine 2%, and FBS 10%. The medium was renewed each third day, and culture was always below 80% of confluence. This was possible to trypsinize and reseed at low density when necessary.

2.4. Preparation of Nanomaterials Stock Solution

To prepare GNPs stock solutions, the same culture medium as for culture maintenance was used avoiding FBS supplementation. Once the stock solution was prepared, it was sonicated for 2 h to homogenize the solution, and it was used immediately after sonication. A vial with the medium was also exposed to the same conditions using it then with the control groups, and for the preparation of the different concentrations of the stock.

2.5. Cytotoxicity Assay

Plates with 96 wells were seeded with HaCaT cells at 1×10^4 cells/well. The microplates were placed inside a CO_2 5% incubator (37 °C, humidified atmosphere). The medium was replaced after 24 h with 100 µL with the different concentrations of each compound, ranging from 0 to 10 µg/mL. To evaluate the toxicity of the compound in the cell line, the different experimental conditions were tested per sextuplicate (n = 6) for 12, and 24 h. The concentrations selected to calculate the EC_{50} were 0.01, 0.05, 0.1, 0.5, 1, 5 and 10 µg/mL at 12 and 24 h. After an incubation period of 12 or 24 h with the compound, cytotoxicity was measured using the (3-(4, 5-dimethylthiazol-2-yl)-2, 5-diphenyl tetrazolium) (MTT) test, incubating the HaCaT cells with the reagent for 5 h and measuring the absorbance at 550 nm, after solubilized the formazan crystals with DMSO. A Varioskan microplate reader was used to it (ThermoScientific, Canada). The background color was subtracted from the final absorbance values by performing the same experiment in parallel but without adding the MTT reagent.

2.6. Proliferation Assay

HaCaT cells were seeded with a density of 5×10^3 cells/well in 96-microplates. Assay culture conditions and stock preparation were the same as following on cytotoxicity, by adding 0.5% FBS to void total starvation of cells. The proliferation activity was measured during 72 and 96 h using two non-cytotoxic concentrations of GNPs (ten-time diluted based on cytotoxicity at 24 h). EGF at a concentration of 15 ng/mL was used as positive control on each proliferation experiment. MTT assay was conducted before the incubation period. Each experimental condition was tested per sextuplicate.

2.7. Gene Expression

Cells were seeded in microplates with 6 wells at 1.5×10^6 cells/well to perform gene expression analysis. The non-cytotoxic concentrations were selected based on results of cytotoxicity at 24 h, and each condition was tested per triplicate. After 24 h of incubation, the supernatant was removed and wells were washed twice with phosphate-buffered saline (PBS) 1×. After that, RNA extraction, cDNA synthesis, and RT-qPCR were carried out. The entire data analysis was performed with the QuantStudioTM Design & Analysis Software (ThermoFisher, Canada). A reference gene was used for data normalization. The primers of the genes that were analyzed in this study are shown in Table A1 of Appendix A. All of them were obtained using Primer-Blast software [19].

2.8. In Vivo Toxicity

A solution of GNPs in autoclaved potassium (K) medium composed of 2.36 g KCl and 3 g NaCl in 1 L of distilled water was prepared in a concentration of 1000 µg/mL. The number of GNPs was first sterilized under UV light radiation for 1 h. After mixing with K medium, the solution was sonicated for 2 h at maximum frequency. After sonication, serial dilutions were carried out in order to prepare concentrations of 800, 500, 400, 300, 200, 100, 50, and 25 µg/mL, considering that the final concentration would be half of the prepared one after mixing these nanomaterial dispersions with the growth medium. The maintenance and propagation of the N2 worms, supplied by the Caenorhabditis Genetics Center (CGC, Minneapolis, MN, USA), were performed on OP50 *Escherichia coli* seeded nematode growth medium (NGM) at 25 °C [20]. The nematodes and their eggs were washed off NGM plates with 5 mL of distilled water and collected in falcon tubes of 15 mL to produce an L1 stage-synchronized *C. elegans* population. The centrifugation of the falcon tubes was performed at 1300 r.p.m. (2209× *g*) for 3 min and the supernatant was removed. The pellets of *C. elegans*' were resuspended in 100 µL of deuterated water (dH_2O) and placed in Eppendorf tubes with 700 µL of a bleaching solution at 5%. Subsequently, incubation for 15 min while vortexing every 2 min was carried out. After that, centrifugation of the Eppendorf tubes was performed at 700× *g* for 3 min. The supernatant was removed and washing of the pellets was carried out three times in 800 µL of dH_2O. Subsequently, the pellets were resuspended in 100 µL of dH_2O and introduced in NGM plates seeded with 100 µL of an OP50 *E. coli* culture. Egg incubation was carried out for 72 h at 25 °C. To pellet the L1 staged populations, centrifugation at 1300 r.p.m. (2209× *g*) for 3 min was performed, and, after that, it was resuspended in 3 mL of K medium. Plates with 48 wells were utilized to have wells with 62.5 µL of a 1:250 suspension of cholesterol (5 mg/mL in ethyl alcohol) in sterile K medium, 62.5 µL of a 50× concentrated OP50 *E. coli* culture with an optical density of 0.9, pelleted by centrifugation at 4000 r.p.m. (6797× *g*) for 10 min and resuspended in K medium, 115 µL of K medium and 250 µL of the pertinent GNPs solution. A volume of K medium with 50–100 nematodes was then added. Parafilm was used to seal 48-well plates that were placed in an orbital shaker at 25 °C and 120 r.p.m. for 24 h, to study acute toxicity, or 72 h, to study chronic toxicity. After, mixing the GNPs dispersions with the growth medium, the final concentrations of the nanomaterials studied in this experiment were 500, 400, 250, 200, 150, 100, 50, 25, and 12.5 µg/mL. In the plates with 48 wells, the volume of each well was divided into 10 drops of 50 µL to be evaluated under a light microscope (Motic BA410E including Moticam 580 5.0 MP) and thus count the number of living and dead *C. elegans* worms. The survival rate of the nematodes was also measured in the medium and in a toxic zinc chloride (1000 µM) solution as a positive and negative control, respectively. These assays were performed in quintuplicate to ensure reproducible results.

2.9. Statistical Analysis

The one-way analysis of variance (ANOVA) with Tukey's post-hoc analysis was employed to determine the significant differences in this study. The median effective concentration (EC_{50}) was determined by Probit analysis. The statistical GraphPad Prism software version 6 was utilized with a minimum significance of $p < 0.05$.

3. Results and Discussion

3.1. Material Characterization

The transmission electron microscopy images of the GNPs at two magnifications are shown in Figure 1.

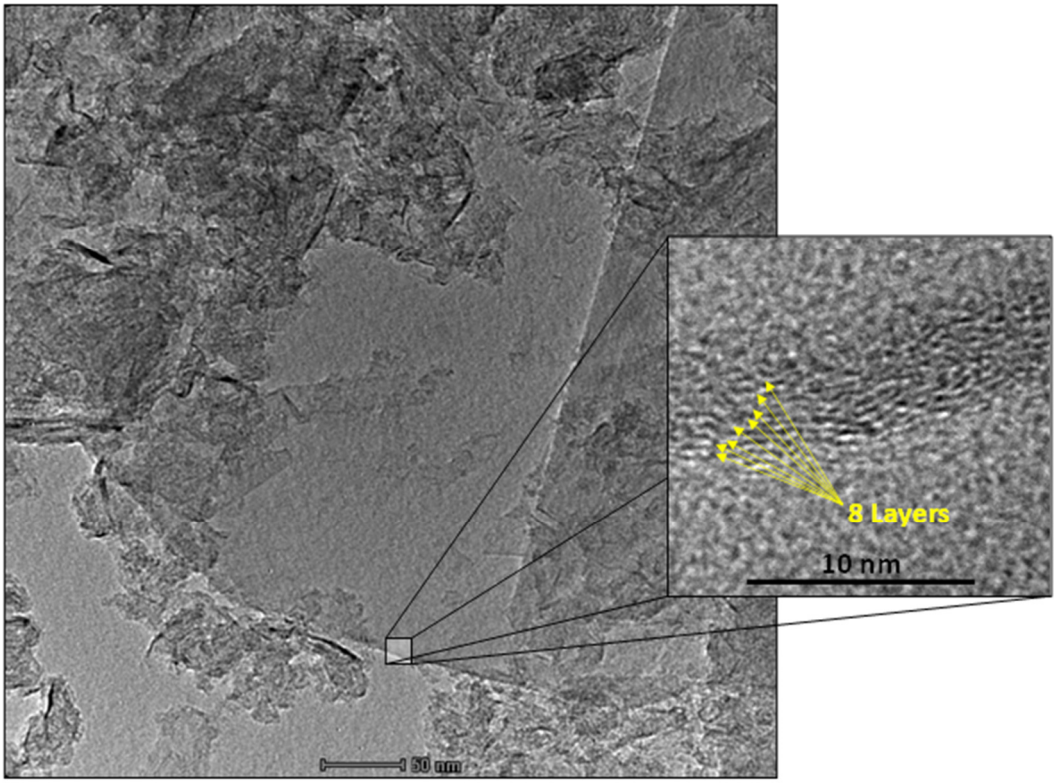

Figure 1. Transmission electron micrographs of graphene nanoplatelets (GNPs). The enlarged image shows the 8 layers of these GNPs.

TEM images show the predominance of GNP agglomerate with sizes ranging between 12 and 97 nm. Furthermore, these GNPs fit as graphene-based materials (GBMs), having a thickness between 2 and 10 layers (Figure 1) according to the European GRAPHENE Flagship Project for the classification of GBMs [21]. The zeta potential (ζ) values of the GNPs are shown in Table 1 as a function of pH, with negative results between pH 5 and 12.

Table 1. Zeta potential (ζ) in mV versus pH of graphene nanoplatelets (GNPs) in water solution.

pH	GNPs
12	−38, 6
10	−33, 2
7	−20, 9
5	−2, 13
3	2, 69

The DLS values (Table 2) show that the rate of aggregation of particles in solution depends on the preparation of the nanofluid with an aqueous solution or DMEM as expected [22].

Table 2. Dynamic light scattering (DLS) particle sizes in nm and polydispersity index (PdI) values of the GNPs in water and in Dulbecco's modified Eagle medium (DMEM).

Material	DLS (nm)		PdI	
	Water	DMEM	Water	DMEM
GNPs	625, 8	2042	0, 557	0, 137

The GNPs show different PdI values in DMEM than in water, which could explain the different DLS sizes determined in bod fluids. These high differences in particle sizes found

in DMEM and water must be related to components present in DMEM that facilitate the aggregation rate, as well as the formation of corona in the particles [23].

The Raman spectrum of the GNPs is shown in Figure 2.

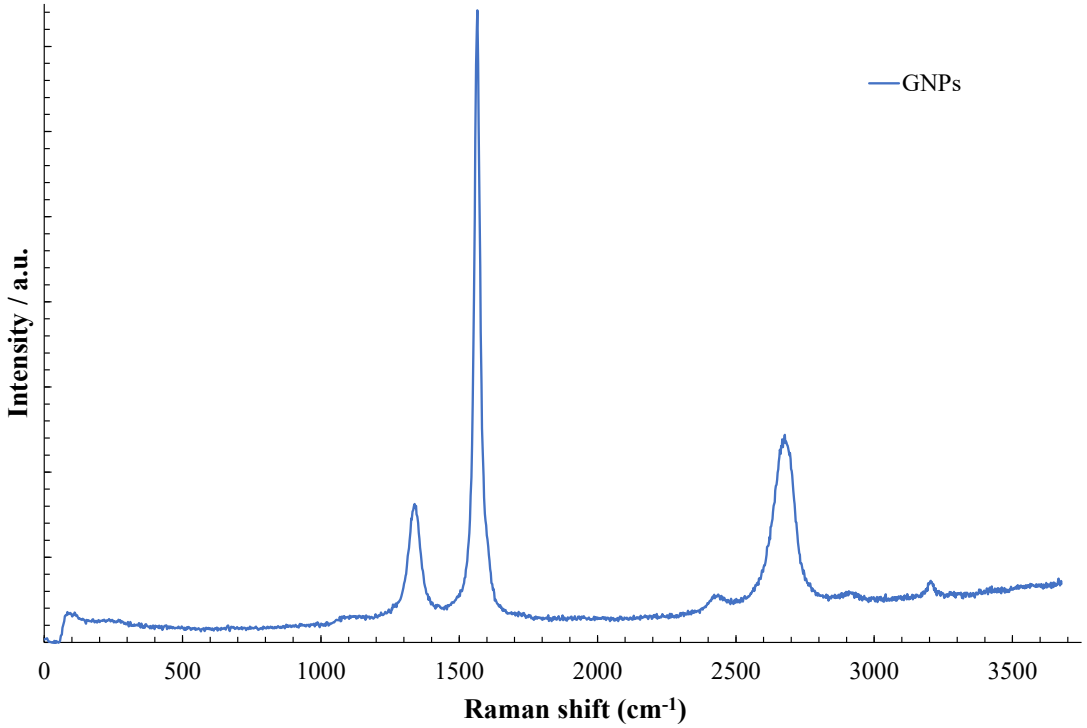

Figure 2. Rama spectrum of graphene nanoplatelets.

The Raman spectroscopy shown in Figure 2 can be used to define the defects of GNPs [24]. The D band, located at 1351 cm^{-1}, refers to defects located in graphene, and the G band, located at 1578 cm^{-1}, is related to sp^2 hybridized carbon bonds ordered in the graphene lattice [25]. Thus, the relation of the intensity of the D band with the G band (I_D/I_G) is related to the degree of defects in this material. The I_D/I_G value of the GNPs was 0.11, indicating the structural quality of the GNPs [24]. The position of the 2D band, for smaller values (in this case 2676 cm^{-1}), also indicates that the material has few layers of graphene sheets in its composition, as indicated in the HR-TEM images [26].

3.2. Cytotoxicity Assay

The cytotoxicity of GNPs in human keratinocytes cells for two different exposure periods (12 and 24 h) and concentrations from 0 (control) to 10 µg/mL were studied. Thus, at 12 h of exposure, higher concentrations of 0.05 µg/mL GNPs showed significant cytotoxic effects in the HaCaT cell line (Figure 3).

The cytotoxicity results at 24 h-exposure of GNPs in HaCaT cells showed also significant non-cytotoxicity for concentrations $\leq$ 0.05 µg/mL (Figure 4).

These results performed at different exposure times clearly shows that the principal cytotoxic effect occurs during the first 12 h. The cell viability of the HaCaT cells after exposure for 12 and 24 h to a GNP concentration of 0.1 µg/mL also showed cell viability higher than 70% indicating non-cytotoxicity according to the ISO-10993 standard (Figures 3 and 4). Studies based on bronchial epithelial cell line (BEAS-2B) cytotoxicity showed similar results at 24 h of cell exposure with GNPs [27].

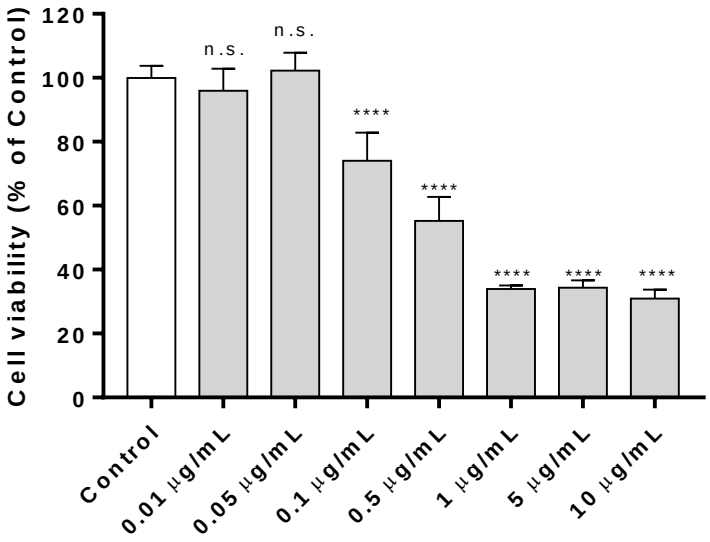

Figure 3. Human keratinocyte HaCaT cell viability after 12 h exposure to GNPs at different concentrations (from 0 µg/mL (control sample) to 10 µg/mL) measured by the (3-(4, 5-dimethylthiazol-2-yl)-2, 5-diphenyl tetrazolium) (MTT) assay. Results are expressed as % of the control sample and as the mean ± standard deviation of six replicates. The results of the statistical analysis with respect to control are indicated in the graph: **** $p < 0.0001$; n.s: not significant. The limit is 70% of cell viability for the materials to be considered non-cytotoxic according to the ISO-10993 standard.

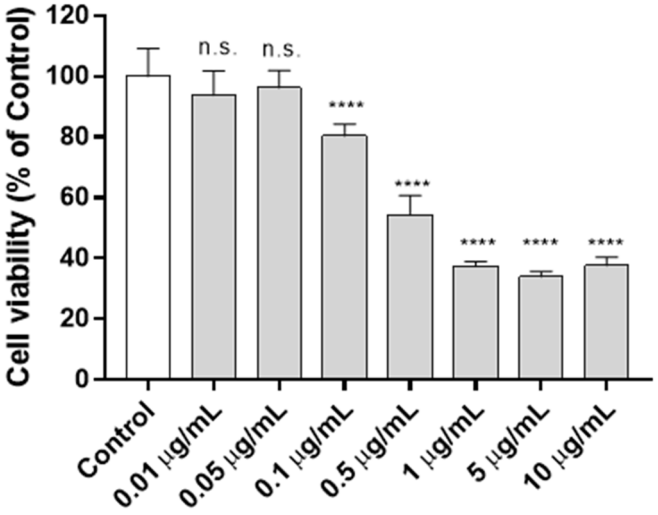

Figure 4. Human keratinocyte HaCaT cell viability after 24 h exposure to GNPs at different concentrations (from 0 µg/mL (control sample) to 10 µg/mL) measured by the (3-(4, 5-dimethylthiazol-2-yl)-2, 5-diphenyl tetrazolium) (MTT) assay. Results are expressed as % of the control sample and as the mean ± standard deviation of six replicates. The results of the statistical analysis with respect to control are indicated in the graph: **** $p < 0.0001$; n.s: not significant. The limit is 70% of cell viability for the materials to be considered non-cytotoxic according to the ISO-10993 standard.

From these results performed at 12 and 24 h of exposure (Figures 3 and 4), the EC_{50} was calculated for the GNPs (Table 3).

Table 3 shows that these non-oxidized CBNs are about five times higher cytotoxic than the oxidized GO nanosheets [13]. This fact can be attributed to smaller sizes of the GO nanosheets used in that study and the hydrophilic functional groups present on their basal planes and at the edges, which decreases toxicity according to previous studies performed with other graphene-based materials [28]. Thus, small and hydrophilic graphene-based

nanomaterials form more stable dispersions significantly reducing aggregation, which can render easier the internalization and excretion cell processes.

Table 3. Median effective concentration (EC_{50}) in μg/mL of keratinocytes (HaCaT) treated with GNPs for 12 and 24 h. Confidence limits (95% CI) and goodness of fitness (R square) are also presented.

Exposure (h)	EC_{50} (μg/mL)	95% CI	R Square
12	1.142	0.837–1.564	0.8961
24	0.760	0.585–1.004	0.9176

3.3. Proliferation Assay

The proliferative activity of GNPs in the keratinocytes cell line was studied with the lowest two non-toxic concentrations (0.005 and 0.01 μg/mL) observed at 24 h (Figure 4) to avoid any increase of toxicity by increasing the treatment time to 72 or 96 h (Figure 5).

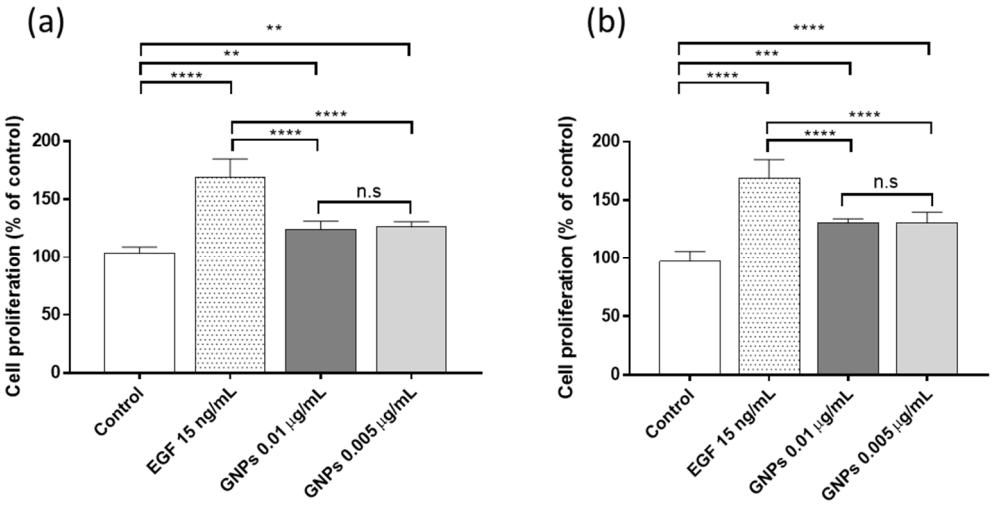

Figure 5. Proliferative activity of GNPs in human keratinocyte HaCaT cells treated with graphene nanoplatelets (GNPs) at non-cytotoxic concentrations (0.005 and 0.01 μg/mL) for 72 (**a**) or 96 (**b**) h. Data are expressed as the mean ± standard deviation of six replicates. The results of the statistical analysis with respect to control and to the epidermal growth factor (EGF) are indicated in the graph: ** $p < 0.01$; *** $p < 0.001$; **** $p < 0.0001$; n.s: not significant.

Although the GNPs showed lower proliferative activity than the EGF growth factor, both non-cytotoxic concentrations of GNPs showed a significant increase of proliferation with respect to control at 72 and 96 h of exposure. It is important to remark that the required exposure time (72 h) to induce proliferation in human keratinocyte HaCaT cells for the GNPs was lower than the 96-h necessary for other nanomaterials such as carbon nanofibers or silver nanoparticles [13]. Proliferative capacity was demonstrated also in GNPs/calcium silicate composites, showing a synergic effect of both components after different periods of exposition to human osteoblast cells [29]. However, the proliferative activity of GNPs in pure state against HaCaT cells is reported here for the first time.

3.4. Gene Expression

The effect of GNPs on the expression of thirteen genes (genes *SOD1*, *CAT*, *MMP1*, *TGFB1*, *GPX1*, *FN1*, *HAS2*, *LAMB1*, *LUM*, *CDH1*, *COL4A1*, *FBN* and *VCAN*) in human keratinocytes cells at two non-cytotoxic concentrations (0.005 and 0.01 μg/mL) exposed for 24 h are shown in Figure 6.

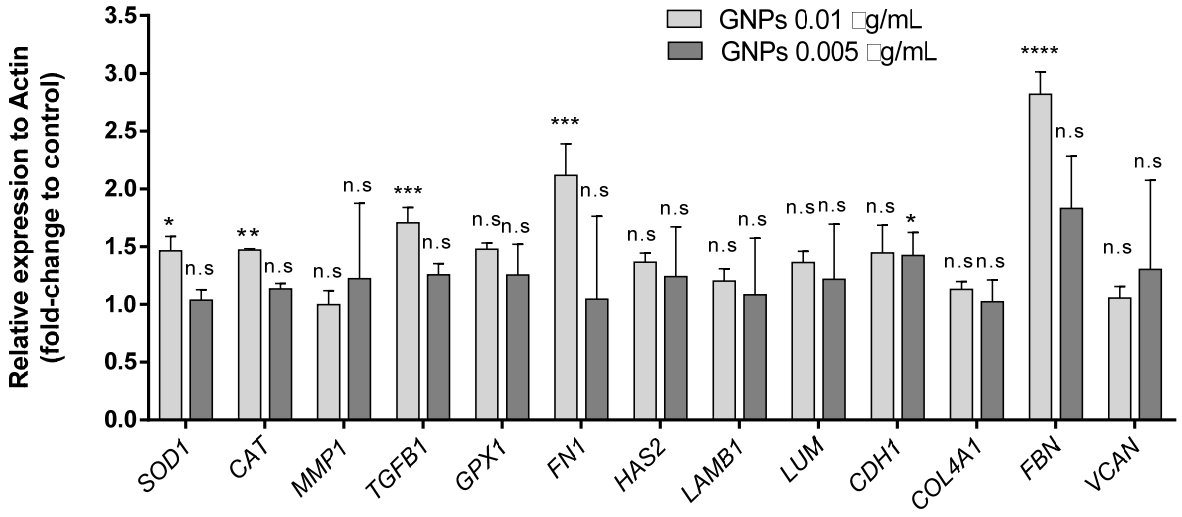

Figure 6. Gene expression in human keratinocyte HaCaT cells exposed at two non-cytotoxic concentrations (0.005 and 0.01 μg/mL) of graphene nanoplatelets (GNPs) for 24 h. Data are shown as mean ± standard deviation from three replicates. Thirteen genes (*SOD1*, *CAT*, *MMP1*, *TGFB1*, *GPX1*, *FN1*, *HAS2*, *LAMB1*, *LUM*, *CDH1*, *COL4A1*, *FBN*, and *VCAN*) are analyzed. The results of the statistical analysis are presented as fold-change of control and relative expression to actin beta (ACTB). * $p < 0.05$; ** $p < 0.01$; *** $p < 0.001$, **** $p < 0.0001$, n.s: not significant.

Figure 6 shows that GNPs can up-regulate the expression of six genes in HaCaT cells (*SOD1*, *CAT*, *TGFB1*, *FN1*, *CDH1*, and *FBN*) in human keratinocytes cells after 24 h.

Thus, multi-layer graphene, GNPs, are able to up-regulate two more genes (*SOD1* and *FBN*) than multi-layer graphene oxide, GO, at 0.01 μg/mL in human keratinocytes [13]. The *SOD1* gene encodes an isozyme that binds copper and zinc ions destroying free superoxide radicals [30]. The expression increases of *FBN* enhance the skin structure and firmness [31]. Therefore, these results reinforce the idea of using these nanomaterials for biomedical applications such as wound healing and skin tissue engineering. Nonetheless, it is important to mention that other carbon materials such as 1D filamentous hollow carbon nanofibers showed effective results in up-regulating eight (*FN1*, *MMP1*, *CAT*, *CDH1*, *COL4A1*, *FBN*, *GPX1*, and *TGFB1*) of the thirteen analyzed genes [14].

Recent studies have tested GNPs not only in keratinocytes but also in mice, the toxicity and activation of inflammatory processes, using the same homogenization technique as in the present study [32]. They concluded that GNPs were not skin sensitizing. Exposure did not induce any type of inflammatory reaction after measuring different interleukins and TNFa, a fact that does not occur in all trials according to the verified bibliography, which does not allow a comparison to be made with our results [33].

3.5. In Vivo Toxicity Test

The *C. elegans* nematode model was used to evaluate in vivo toxicity of the GNPs. The use of this type of in vivo model is very useful and cost-effective for toxicity testing [34]. Furthermore, this nematode shares human proteins, lipids, genes, and signaling ways, and its digestive system possesses many aspects that are similar to those of mammals [17,35–38]. Additionally, *C. elegans*' genomics is used for the study of human development and disease [17]. Besides, it presents not many ethical difficulties. In contrast to cytotoxicity assays, in vivo toxicity tests performed with *C. elegans* provide data from a complete animal [18]. Thus, the survival rate of the worms was analyzed after an exposure of 24 h (acute toxicity) and 72 h (chronic toxicity) to several concentrations of GNPs ranging from 12.5 to 500 μg/mL (see Figure 7).

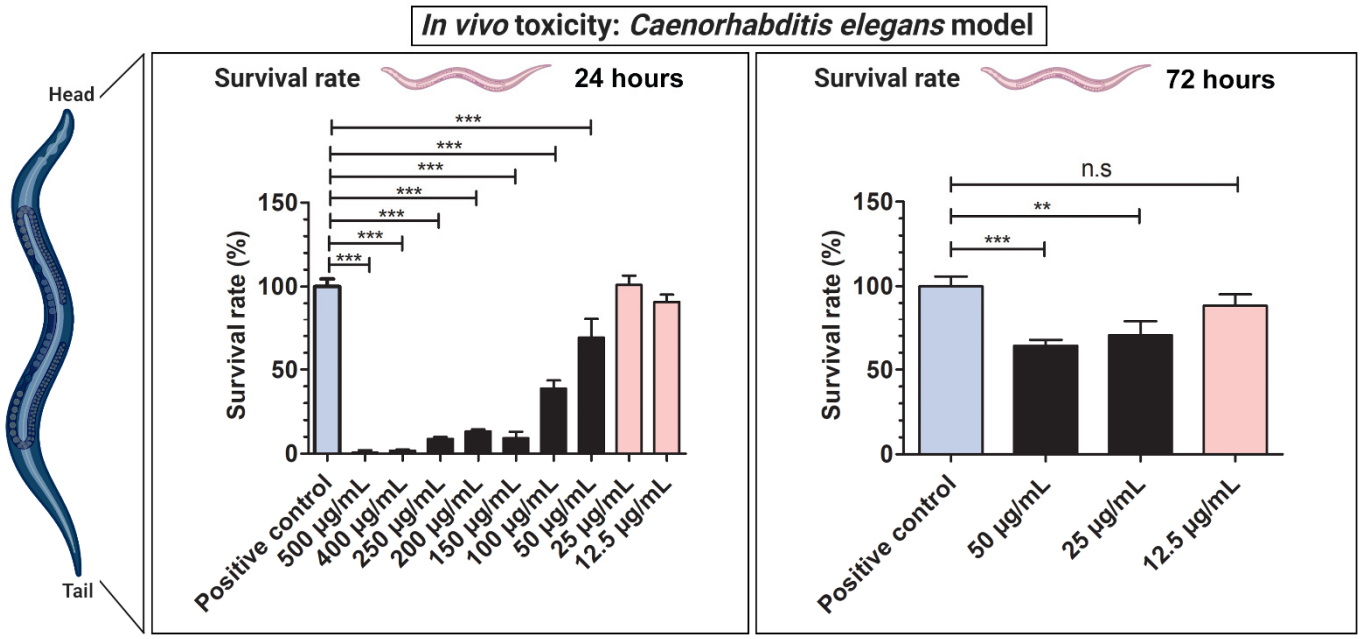

Figure 7. Survival rate of the *Caenorhabditis elegans* in vivo toxicity model after 24 h (acute toxicity) and 72 h (chronic toxicity) of exposure to graphene nanoplatelets (GNPs). Data are expressed as the mean ± standard deviation of five replicates (n = 5). The results of the statistical analysis with respect to positive control and to the epidermal growth factor (EGF) are indicated in the graph: ** $p < 0.01$; *** $p < 0.001$, n.s: not significant.

GNPs can be used in vivo at higher non-toxic concentrations as expected. Thus, exposure of *C. elegans* to 25 and 12.5 µg/mL for 24 h showed no significant in vivo toxicity. However, at a higher exposure time of 72 h (chronic toxicity), only a concentration of 12.5 µg/mL of GNPs showed non-cytotoxic effects. Since the concentrations of GNPs at 500, 400, 250, 200, 150, and 100 µg/mL of GNPs show toxic effects at 24 h, the chronic toxicity of these concentrations was not evaluated at 72 h of exposure.

According to the current studies carried out in this emerging research field, the generation of reactive oxygen species (ROS) in target cells is proposed as the most important cytotoxic mechanism of graphene materials [28]. The capacity of cell proliferation and up-regulation of the six genes of human keratinocytes (*SOD1*, *CAT*, *TGFB1*, *FN1*, *CDH1*, and *FBN*) can also be attributed to the ROS generation of the GNPs. However, further studies are necessary to better elucidate the toxicity pathways on a molecular level.

Therefore, GNPs used at non-cytotoxic concentrations are very promising functional two-dimensional materials for biomedical applications.

4. Conclusions

The results of this study show that multi-layer graphene, also called graphene nanoplatelets (GNPs), are carbon-based nanomaterials with great potential in biomedicine and can be summarized as follows: (i) GNPs can be used in vivo at the non-toxic concentrations of 25 and 12.5 µg/mL for 24 h (acute toxicity), and at 12.5 µg/mL for 72 h (chronic toxicity) of exposure in *C. elegans* model; (ii) GNPs present time-dependent cytotoxicity (EC_{50} of 1.142 µg/mL and 0.760 µg/mL at 12 h and 24 h, respectively) in human keratinocyte HaCaT cells; (iii) GNPs showed significant proliferative activity at the non-cytotoxic concentrations of 0.005 and 0.01 µg/mL in the keratinocytes; (iv) The gene expression analysis showed that GNPs are capable of up-regulating six of the thirteen genes (*SOD1*, *CAT*, *TGFB1*, *FN1*, *CDH1*, and *FBN*), which are involved with many important features required in biomedical fields such as wound healing and skin tissue engineering. However, more experimentation is required to provide strong scientific conclusions about the potential biomedical use of these materials in humans.

Author Contributions: Conceptualization: B.S. and Á.S.-A.; methodology, validation, and formal analysis: B.S., A.T.-M., A.C.-V., M.A., J.A. and Á.S.-A.; software: B.S. and Á.S.-A.; investigation: B.S., A.T.-M., A.C.-V., M.A., J.A. and Á.S.-A.; resources: J.A. and Á.S.-A.; data curation: B.S., A.T.-M., A.C.-V., M.A., J.A. and Á.S.-A.; visualization: B.S. and Á.S.-A.; writing—original draft preparation: Á.S.-A.; writing—review and editing: B.S., A.T.-M., A.C.-V., M.A., J.A. and Á.S.-A.; supervision: J.A. and Á.S.-A.; project administration: Á.S.-A.; funding acquisition, J.A. and Á.S.-A. All authors have read and agreed to the published version of the manuscript.

Funding: This research was supported by the Fundación Universidad Católica de Valencia San Vicente Mártir, Grant 2020-231-006UCV and by the Ministerio de Ciencia e Innovación (PID2020-119333RB-I00/AEI/10.13039/501100011033) (awarded to Á.S-A). J.A. acknowledges Universitat Jaume I for project UJI-B2019-30, Generalitat Valenciana for project AICO2020, and Ministerio de Ciencia, Innovación y Universidades (Spain) project PGC2018- 094417-B-I00 for supporting this research financially. M.A. acknowledges Fundação de Amparo à Pesquisa do Estado de São Paulo—FAPESP (FAPESP CEPID-finance code 2013/07296-2), FINEP, Conselho Nacional de Desenvolvimento Cientifico e Tecnológico—CNPq (finance code 166281/2017-4), and CAPES (finance code 001).

Institutional Review Board Statement: Not applicable.

Informed Consent Statement: Not applicable.

Data Availability Statement: Data is contained within the article.

Acknowledgments: The authors would like to express their gratitude to the Fundación Universidad Católica de Valencia San Vicente Mártir, the Generalitat Valenciana, the Fundação de Amparo à Pesquisa do Estado de São Paulo and to the Spanish Ministry of Science and Innovation for their financial support.

Conflicts of Interest: The authors declare no conflict of interest.

Appendix A

Table A1. Gene symbol, gene name, oligo sequences and function of gene-specific [19] used in RTqPCR measurements.

Gene Symbol (Access Number)	Gene Name	Oligo Sequences	Function
ACTB (NM_001101)	Actin beta	5′-CCATGCCCACCATCACGC-3′ 5′-CACAGAGCCTCGCCTTTG-3′	Highly conserved protein that is involved in cell motility, structure, and integrity
CAT (NM_001752)	Catalase	5′-TGAATGAGGAACAGAGGAAACG-3′ 5′-AGATCCGGACTGCACAAAG-3′	Encodes catalase, a key antioxidant enzyme in the bodies defence against oxidative stress
CDH1 (NM_001317184)	Cadherin 1	5′-AACAGCACGTACACAGCCCT-3′ 5′-TCTGGTATGGGGGCGTTGTC-3′	Loss of function of this gene is thought to contribute to cancer progression by increasing proliferation, invasion, and/or metastasis.
COL4A1 (NM_000088)	Collagen type I alpha 1	5′-CAAGGGCGACAGAGGTTTGC-3′ 5′-AAAACTCACCAGGCTCCCCC-3′	Abundant in bone, cornea, dermis, and tendon. Mutations in this gene are associated with osteogenesis imperfect types I-IV
FBN (NM_000138)	Fibrillin 1	5′-ATCCAACCACGTGCATCAGT-3′ 5′-AGAGCGGGTATCAACACAGC-3′	Extracellular matrix glycoprotein that is useful as a structural component of calcium-binding microfibrils, providing force-bearing structural support in elastic and nonelastic connective tissue throughout the body
FN1 (NM_001306129)	Fibronectin 1	5′-GGCCAGTCCTACAACCAGT-3′ 5′-CGGGAATCTTCTCTGTCAGC-3′	Involved in cell adhesion and migration processes including embryogenesis, wound healing, blood coagulation, host defence and metastasis.

Table A1. *Cont.*

Gene Symbol (Access Number)	Gene Name	Oligo Sequences	Function
GPX1 (NM_000581)	Glutathione peroxidase 1	5′-TTTGGGCATCAGGAGAACGC-3′ 5′-ACCGTTCACCTCGCACTTC-3′	Catalyse the reduction of organic hydroperoxides and hydrogen peroxide by glutathione, and thereby protect cells against oxidative damage
HAS2 (NM_005328)	Hyaluronan synthase 2	5′-CCGAGAATGGCTGTACAATGC-3′ 5′-AGAGCTGGATTACTGTGGCAA-3′	Serves a variety of functions, including space filling, lubrication of joints, and provision of a matrix through which cells can migrate
LAMB1 (NM_002291)	Laminin subunit beta 1	5′-CAGGGTGTGCAGTCAGGGAA-3′ 5′-TGTGTCTGCGTTGAGGGTGT-3′	Implicated in a wide variety of biological processes including cell adhesion, differentiation, migration, signalling, neurite outgrowth and metastasis
LUM (NM_002345)	Lumican	5′-ACTTGGGTAGCTTTCAGGGCA-3′ 5′-TTCCTGGCATTGATTGGTGGT-3′	Is the major keratan sulfate proteoglycan of the cornea but is also distributed in interstitial collagenous matrices throughout the body
MMP1 (NM_001145938)	Matrix metallopeptidase 1	5′-GGACCATGCCATTGAGAAAG-3′ 5′-TCCTCCAGGTCCATCAAAAG-3′	Involved in the breakdown of extracellular matrix in normal physiological processes
SOD1 (NM_000454)	Superoxide dismutase 1	5′-GGTGTGGCCGATGTGTCT-3′ 5′-TCCACCTTTGCCCAAGTCA-3′	The protein encoded by this gene binds to Cu^{2+} and Zn^{2+} cations and is one of two isozymes capable of destroying free superoxide radicals in the body
TGFB1 (NM_000660)	Transforming growth factor beta 1	5′-AGCTGTACATTGACTTCCGCA-3′ 5′-TGTCCAGGCTCCAAATGTAGG-3′	Regulates cell proliferation, differentiation, and growth
VCAN (NM_001126336)	Versican	5′-CTGGTCTCCGCTGTATCCTG-3′ 5′-ATCGCTGCAAAATGAACCCG-3′	Involved in cell adhesion, proliferation, migration, and angiogenesis and plays a central role in the morphogenesis and maintenance of tissue

References

1. Sportelli, M.C.; Izzi, M.; Kukushkina, E.A.; Hossain, S.I.; Picca, R.A.; Ditaranto, N.; Cioff, N. Can nanotechnology and materials science help the fight against SARS-CoV-2? *Nanomaterials* **2020**, *10*, 802. [CrossRef]
2. Weiss, C.; Carriere, M.; Fusco, L.; Fusco, L.; Capua, I.; Regla-Nava, J.A.; Pasquali, M.; Pasquali, M.; Pasquali, M.; Scott, J.A.; et al. Toward Nanotechnology-Enabled Approaches against the COVID-19 Pandemic. *ACS Nano* **2020**, *14*, 6383–6406. [CrossRef] [PubMed]
3. Ruiz-Hitzky, E.; Darder, M.; Wicklein, B.; Ruiz-Garcia, C.; Martín-Sampedro, R.; del Real, G.; Aranda, P. Nanotechnology Responses to COVID-19. *Adv. Healthc. Mater.* **2020**, *9*, 2000979.
4. Serrano-Aroca, Á.; Takayama, K.; Tuñón-Molina, A.; Seyran, M.; Hassan, S.S.; Pal Choudhury, P.; Uversky, V.N.; Lundstrom, K.; Adadi, P.; Palù, G.; et al. Carbon-Based Nanomaterials: Promising Antiviral Agents to Combat COVID-19 in the Microbial-Resistant Era. *ACS Nano* **2021**, *15*, 8069–8086. [CrossRef]
5. Zou, X.; Zhang, L.; Wang, Z.; Luo, Y. Mechanisms of the Antimicrobial Activities of Graphene Materials. *J. Am. Chem. Soc.* **2016**, *138*, 2064–2077. [CrossRef]
6. Salesa, B.; Llorens-Gámez, M.; Serrano-Aroca, Á. Study of 1D and 2D carbon nanomaterial in alginate films. *Nanomaterials* **2020**, *10*, 206. [CrossRef]
7. Gardea, F.; Naraghi, M.; Lagoudas, D. Effect of thermal interface on heat flow in carbon nanofiber composites. *ACS Appl. Mater. Interfaces* **2014**, *6*, 1061–1072. [CrossRef]
8. Tran, P.A.; Zhang, L.; Webster, T.J. Carbon nanofibers and carbon nanotubes in regenerative medicine. *Adv. Drug Deliv. Rev.* **2009**, *61*, 1097–1114. [PubMed]
9. Sanmartín-Santos, I.; Gandía-Llop, S.; Salesa, B.; Martí, M.; Aachmann, F.L.; Serrano-Aroca, Á. Enhancement of Antimicrobial Activity of Alginate Films with a Low Amount of Carbon Nanofibers (0.1% w/w). *Appl. Sci.* **2021**, *11*, 2311. [CrossRef]
10. Geim, A.K. Graphene: Status and prospects. *Science* **2009**, *324*, 1530–1534.
11. Henriques, P.C.; Borges, I.; Pinto, A.M.; Magalhães, F.D.; Gonçalves, I.C. Fabrication and antimicrobial performance of surfaces integrating graphene-based materials. *Carbon* **2018**, *132*, 709–732.

12. Pelin, M.; Fusco, L.; León, V.; Martín, C.; Criado, A.; Sosa, S.; Vázquez, E.; Tubaro, A.; Prato, M. Differential cytotoxic effects of graphene and graphene oxide on skin keratinocytes. *Sci. Rep.* **2017**, *7*, 40572. [CrossRef] [PubMed]
13. Salesa, B.; Serrano-Aroca, Á. Multi-Layer Graphene Oxide in Human Keratinocytes: Time-Dependent Cytotoxicity, Proliferation, and Gene Expression. *Coatings* **2021**, *11*, 414. [CrossRef]
14. Salesa, B.; Assis, M.; Andrés, J.; Serrano-Aroca, Á. Carbon Nanofibers versus Silver Nanoparticles: Time-Dependent Cytotoxicity, Proliferation, and Gene Expression. *Biomedicines* **2021**, *9*, 1155. [CrossRef]
15. Gomes, R.N.; Borges, I.; Pereira, A.T.; Maia, A.F.; Pestana, M.; Magalhães, F.D.; Pinto, A.M.; Gonçalves, I.C. Antimicrobial graphene nanoplatelets coatings for silicone catheters. *Carbon* **2018**, *139*, 635–647. [CrossRef]
16. Chieng, B.W.; Ibrahim, N.A.; Yunus, W.M.Z.W.; Hussein, M.Z.; Then, Y.Y.; Loo, Y.Y. Reinforcement of graphene nanoplatelets on plasticized poly(lactic acid) nanocomposites: Mechanical, thermal, morphology, and antibacterial properties. *J. Appl. Polym. Sci.* **2015**, *132*, 41652. [CrossRef]
17. Kuwabara, P.E.; O'Neil, N. The use of functional genomics in C. elegans for studying human development and disease. *J. Inherit. Metab. Dis.* **2001**, *24*, 127–138. [CrossRef]
18. Yin, J.; Hong, X.; Ma, L.; Liu, R.; Bu, Y. Non-targeted metabolomic profiling of atrazine in Caenorhabditis elegans using UHPLC-QE Orbitrap/MS. *Ecotoxicol. Environ. Saf.* **2020**, *206*, 111170. [CrossRef]
19. NCBI Primer Designing Tool. Available online: https://www.ncbi.nlm.nih.gov/tools/primer-blast/ (accessed on 5 August 2021).
20. Stiernagle, T. Maintenance of *C. elegans*, WormBook, ed. The *C. elegans* Research Community, WormBook. 2006. Available online: http://www.wormbook.org (accessed on 12 December 2021). [CrossRef]
21. Wick, P.; Louw-Gaume, A.E.; Kucki, M.; Krug, H.F.; Kostarelos, K.; Fadeel, B.; Dawson, K.A.; Salvati, A.; Vázquez, E.; Ballerini, L.; et al. Classification framework for graphene-based materials. *Angew. Chem. Int. Ed.* **2014**, *53*, 7714–7718.
22. Aguilar, T.; Sani, E.; Mercatelli, L.; Carrillo-Berdugo, I.; Torres, E.; Navas, J. Exfoliated graphene oxide-based nanofluids with enhanced thermal and optical properties for solar collectors in concentrating solar power. *J. Mol. Liq.* **2020**, *306*, 112862. [CrossRef]
23. Franqui, L.S.; De Farias, M.A.; Portugal, R.V.; Costa, C.A.R.; Domingues, R.R.; Souza Filho, A.G.; Coluci, V.R.; Leme, A.F.P.; Martinez, D.S.T. Interaction of graphene oxide with cell culture medium: Evaluating the fetal bovine serum protein corona formation towards in vitro nanotoxicity assessment and nanobiointeractions. *Mater. Sci. Eng. C* **2019**, *100*, 363–377. [CrossRef]
24. Zhang, K.; Zhang, X.; Li, H.; Xing, X.; Jin, L.; Cao, Q.; Li, P. Direct exfoliation of graphite into graphene in aqueous solution using a novel surfactant obtained from used engine oil. *J. Mater. Sci.* **2018**, *53*, 2484–2496. [CrossRef]
25. Skaltsas, T.; Ke, X.; Bittencourt, C.; Tagmatarchis, N. Ultrasonication induces oxygenated species and defects onto exfoliated graphene. *J. Phys. Chem. C* **2013**, *117*, 23272–23278. [CrossRef]
26. Zhang, L.; Zhang, Z.; He, C.; Dai, L.; Liu, J.; Wang, L. Rationally designed surfactants for few-layered graphene exfoliation: Ionic groups attached to electron-deficient π-conjugated unit through alkyl spacers. *ACS Nano* **2014**, *8*, 6663–6670. [CrossRef]
27. Park, E.J.; Lee, G.H.; Han, B.S.; Lee, B.S.; Lee, S.; Cho, M.H.; Kim, J.H.; Kim, D.W. Toxic response of graphene nanoplatelets in vivo and in vitro. *Arch. Toxicol.* **2015**, *89*, 1557–1568. [CrossRef]
28. Seabra, A.B.; Paula, A.J.; De Lima, R.; Alves, O.L.; Durán, N. Nanotoxicity of graphene and graphene oxide. *Chem. Res. Toxicol.* **2014**, *27*, 159–168. [PubMed]
29. Mehrali, M.; Moghaddam, E.; Shirazi, S.F.S.; Baradaran, S.; Mehrali, M.; Latibari, S.T.; Metselaar, H.S.C.; Kadri, N.A.; Zandi, K.; Osman, N.A.A. Mechanical and in vitro biological performance of graphene nanoplatelets reinforced calcium silicate composite. *PLoS ONE* **2014**, *9*, e106802. [CrossRef]
30. Chen, D.; Lu, Y.; Yu, W.; Luo, J.; Xiao, Z.; Xiao, F.; Wang, X. Clinical value of decreased superoxide dismutase 1 in patients with epilepsy. *Seizure* **2012**, *21*, 508–511. [CrossRef]
31. Philips, N.; Samuel, M.; Arena, R.; Chen, Y.J.; Conte, J.; Natrajan, P.; Haas, G.; Gonzalez, S. Direct inhibition of elastase and matrixmetalloproteinases and stimulation of biosynthesis of fibrillar collagens, elastin, and fibrillins by xanthohumol. *J. Cosmet. Sci.* **2010**, *61*, 125–132. [CrossRef]
32. Kim, S.H.; Hong, S.H.; Lee, J.H.; Lee, D.H.; Jung, K.; Yang, J.Y.; Shin, H.S.; Lee, J.; Jeong, J.; Oh, J.H. Skin sensitization evaluation of carbon-based graphene nanoplatelets. *Toxics* **2021**, *9*, 62. [CrossRef]
33. Domenech, J.; Hernández, A.; Demir, E.; Marcos, R.; Cortés, C. Interactions of graphene oxide and graphene nanoplatelets with the in vitro Caco-2/HT29 model of intestinal barrier. *Sci. Rep.* **2020**, *10*, 2793. [CrossRef]
34. Hunt, P.R. The C. elegans model in toxicity testing. *J. Appl. Toxicol.* **2017**, *37*, 50–59. [PubMed]
35. Sonnhammer, E.L.L.; Durbin, R. Analysis of Protein Domain Families inCaenorhabditis elegans. *Genomics* **1997**, *46*, 200–216. [CrossRef] [PubMed]
36. Chauhan, V.M.; Orsi, G.; Brown, A.; Pritchard, D.I.; Aylott, J.W. Mapping the pharyngeal and intestinal pH of Caenorhabditis elegans and real-time luminal pH oscillations using extended dynamic range pH-sensitive nanosensors. *ACS Nano* **2013**, *7*, 5577–5587. [CrossRef] [PubMed]
37. Stutz, K.; Kaech, A.; Aebi, M.; Künzler, M.; Hengartner, M.O. Disruption of the C. elegans Intestinal Brush Border by the Fungal Lectin CCL2 Phenocopies Dietary Lectin Toxicity in Mammals. *PLoS ONE* **2015**, *10*, e0129381. [CrossRef]
38. Zhang, Y.; Zou, X.; Ding, Y.; Wang, H.; Wu, X.; Liang, B. Comparative genomics and functional study of lipid metabolic genes in Caenorhabditis elegans. *BMC Genom.* **2013**, *14*, 164. [CrossRef]